Comparison of Lamina Cribrosa Morphology in Normal Tension Glaucoma and Autosomal-Dominant Optic Atrophy

Gyu-Nam Kim,[1] Ji-Ah Kim,[2] Mi-Ji Kim,[3] Eun Ji Lee,[2] Jeong-Min Hwang,[2] and Tae-Woo Kim[2]

[1]Department of Ophthalmology, Institute of Health Sciences, Gyeongsang National University College of Medicine, Gyeongsang National University Hospital, Jinju, South Korea

[2]Department of Ophthalmology, Seoul National University College of Medicine, Seoul National University Bundang Hospital, Seongnam, South Korea

[3]Department of Preventive Medicine, Institute of Health Science, Gyeongsang National University College of Medicine, Jinju, South Korea

PURPOSE. To compare lamina cribrosa (LC) morphology in patients with normal tension glaucoma (NTG) and autosomal-dominant optic atrophy (ADOA).

METHODS. This cross-sectional study matched 24 patients diagnosed with ADOA (24 eyes) by age and retinal nerve fiber layer thickness with 48 patients diagnosed with NTG (48 eyes) by age with 48 healthy controls (48 eyes). Optic nerve heads were scanned by enhanced-depth imaging (EDI) optical coherence tomography (OCT). The LC curvature index (LCCI) and LC depth (LCD) on B-scan images obtained using EDI-OCT were measured at seven locations spaced equidistantly across the vertical optic disc diameter and compared among the NTG, ADOA, and control groups.

RESULTS. Mean LCCI and LCD were significantly greater in NTG than in ADOA and healthy eyes ($P < 0.001$ each) but did not differ significantly in ADOA and healthy eyes.

CONCLUSIONS. NTG eyes have a more posteriorly curved and deeper LC than ADOA and healthy eyes. This finding provides insight into the role of LC morphology in NTG and provides a clinical clue to distinguish between NTG and ADOA.

Keywords: dominant optic atrophy, normal tension glaucoma, lamina cribrosa, lamina cribrosa curve index

Glaucoma, the most common type of acquired optic neuropathy, is characterized by progressive loss of retinal ganglion cells (RGCs) and their axons.[1,2] Another type of progressive optic neuropathy, autosomal-dominant optic atrophy (ADOA), is the most common form of nonglaucomatous hereditary optic neuropathy and is caused by mutations in the *OPA1* gene *OPA1*.[3,4] Patients with ADOA present with progressive bilaterally variable vision loss, central or cecocentral visual field (VF) defects, color vision defects, and temporal or diffuse pallor of the optic disc with optic disc excavation.[5–8]

Although temporal or diffuse pallor of the optic nerve head (ONH) is a characteristic finding of ADOA, most patients with ADOA are also associated with rim loss and excavation of the ONH, with many therefore being misdiagnosed with glaucoma.[9–11] Several additional clinical features may differentiate ADOA from normal tension glaucoma (NTG), including early onset, preferential loss of central vision with relative sparing of the peripheral field, and family history.[9,12] NTG, however, may be diagnosed in younger individuals, including those in their 30s and 40s,[13,14] whereas the onset of visual loss in ADOA may occur after age 60 years.[15] In addition, many NTG patients have a family history of this disease.[16,17] Because of these overlapping features, differential diagnosis may be difficult, even when overall clinical features and optic disc appearance are considered.

The lamina cribrosa (LC) has been regarded as the primary site of pathogenesis in glaucoma.[18] An experimental study in an early glaucoma model showed that morphologic changes in the LC preceded damage to the retinal nerve fiber layer (RNFL).[19,20] Biomechanical changes in the LC are thought to induce damage to axonal and/or RGCs through various mechanisms, including blockade of axonal transport, and tissue remodeling by reactive astrocytes.[21–24] Capillary blood flow disturbance inside the deformed LC can affect the nutrient supply, further compromising the axons.[25,26] In ADOA, however, optic nerve damage results from primary degeneration of the RGC layer.[27–31] It is unclear whether LC deformation is also involved in ADOA, either as a primary event or secondary to RGC degeneration.

Differences in the etiopathogenesis of optic nerve damage in patients with NTG and ADOA suggested that LC morphology may differ in these two conditions. Determining these differences may assist in their differential diagnosis and expand insight into their pathogenesis. The present

study therefore compared LC morphology in patients with NTG and ADOA.

METHODS

This retrospective study included patients who visited Seoul National University Bundang Hospital (SNUBH) from January 2010 to December 2018. The study protocol was approved by the institutional review board of SNUBH and conformed to the tenets of the Declaration of Helsinki. Written informed consent was obtained from all patients.

Study Subjects

All patients underwent a complete ophthalmic examination, including measurements of best corrected visual acuity (BCVA); refraction tests; slit-lamp biomicroscopy; Goldmann applanation tonometry; gonioscopy; dilated stereoscopic examination of the optic disc; measurements of corneal curvature (KR-1800; Topcon, Tokyo, Japan), central corneal thickness (CCT) (Orbscan II; Bausch & Lomb Surgical, Rochester, NY, USA), and axial length (IOL Master version 5; Carl Zeiss Meditec, Dublin, CA, USA); stereo disc photography (EOS D60 digital camera; Canon, Utsunomiya-shi, Tochigi ken, Japan); spectral-domain (SD) optical coherence tomography (OCT) (Spectralis; Heidelberg Engineering, Heidelberg, Germany); and standard automated perimetry (Humphrey Field Analyzer II 750 and 24-2 Swedish interactive threshold algorithm; Carl Zeiss Meditec).

NTG was diagnosed according to the following criteria: intraocular pressure (IOP) $\leq$21 mm Hg on multiple measurements on the same day or over a few days before starting IOP-lowering medication, an open angle on gonioscopy, glaucomatous optic nerve damage (e.g., diffuse or localized rim thinning, notching, or disc hemorrhage), and associated VF defects without ocular disease or conditions that may cause VF abnormalities. A glaucomatous VF change was defined as the fulfillment of two or more of the following criteria: (1) outside normal limits on the glaucoma Hemifield test; (2) three abnormal points with <5% probability of being normal, including one with a probability <1%, by pattern deviation; or (3) a pattern standard deviation of probability <5%. These VF defects were confirmed on two consecutive reliable tests (fixation loss rate $\leq$20%, false-positive and false-negative error rates $\leq$25%).[32]

We included patients with genetic (*OPA1* mutations) or clinical diagnosis of ADOA. Family history was considered for both criteria. Clinical diagnosis of ADOA was based on a history of gradual, bilateral vision loss; dyschromatopsia; a central, cecocentral, or paracentral scotoma; optic disc pallor; and bilaterally symmetric RNFL loss involving the temporal sector.[33] The parents, and when necessary the grandparents, of each patient underwent a complete ophthalmologic examination that included BCVA evaluation, fundus photography, VF examination, and a color test. Any patients with the possibility of optic atrophy of other causes, such as acute visual loss, pain, previous febrile event, drug history, and disc hemorrhage or edema, were excluded.

Healthy control individuals included subjects with an IOP $\leq$21 mm Hg with no history of increased IOP, absence of a glaucomatous disc, a circumpapillary RNFL thickness within the normal range (as measured by SD-OCT), and a normal VF. The absence of a glaucomatous disc was defined as an intact appearing neuroretinal rim without disc hemorrhages,

notches, rim thinning, adjacent RNFL defect, or localized pallor. Two independent glaucoma specialists (G.N.K and J.-A.K) evaluated the optic disc. Disagreements between the observers were resolved by a third adjudicator (T.-W.K.). The normal range of RNFL thickness was defined as a circumpapillary RNFL thickness within the 95th percentile of the normative database, whereas VF was considered normal when there were no glaucomatous VF or neurologic defects.[34,35]

Eyes were excluded if they had a BCVA worse than 20/40, a spherical equivalent less than –6.0 diopter (D) or greater than +3.0 D, a cylinder correction of less than –3.0 D or greater than +3.0 D, a tilted disc (i.e., a tilt ratio >1.3 between the longest and shortest diameters of the optic disc),[36,37] or a torted disc (i.e., a torsion angle deviation of the long axis of the optic disc from the vertical meridian of >15°)[37,38]; a history of intraocular surgery, except for uneventful cataract surgery; or the presence of a retinal or neurologic disease other than ADOA that may affect VF. Eyes were also excluded if a good-quality image (i.e., quality score >15) could not be obtained in more than five sections; if this quality score was not attained, the image-acquisition process automatically stopped, or images of the respective sections were not obtained. LC depth (LCD) and LC curvature index (LCCI) were measured only on acceptable scans with good-quality images that allowed clear delineation of the anterior border of the LC within the Bruch's membrane opening (BMO).

Enhanced-Depth Imaging (EDI)-OCT of the ONH and Adaptive Compensation

LCD and LCCI were measured on optic disc B-scan images, which were obtained using the EDI technique of the SD-OCT system with a high-speed setting.[39] Prior to disc scanning, the corneal curvature of each eye was entered into the Spectralis OCT system to avoid potential magnification errors. The optic disc was imaged through undilated pupils using a rectangle subtending 10° X 15° of the optic disc. This rectangle was scanned with approximately 75 B-scan section images separated by 30 to 34 µm, with the distance between the scan lines determined automatically. An average 42 SD-OCT frames were obtained for each section. This protocol provided the best trade-off between image quality and patient cooperation.[40] To enhance the visibility of the anterior LC surface, all disc scan images were postprocessed by adaptive compensation,[41–43] and the measurements were performed using a manual caliper tool in the software (Amira, version 5.2.2; Visage Imaging, Berlin, Germany) by two experienced observers (G.N.K. and J.-A.K.) who were masked to the clinical information. If the anterior LC surface was not visualized clearly, an adjacent horizontal EDI-OCT scan, approximately 30 to 35 µm from the original scan, was used for measurement. If the anterior LC surface could also not be visualized on the adjacent scans, that eye was excluded. The average LCD and LCCI were the means of the measurements taken at seven points of the LC. The mean of the measurements taken by the two observers were used for analysis.

Measurement of LCD

LCDs on horizontal SD-OCT B-scan images were measured at seven locations equidistant across the vertical optic disc
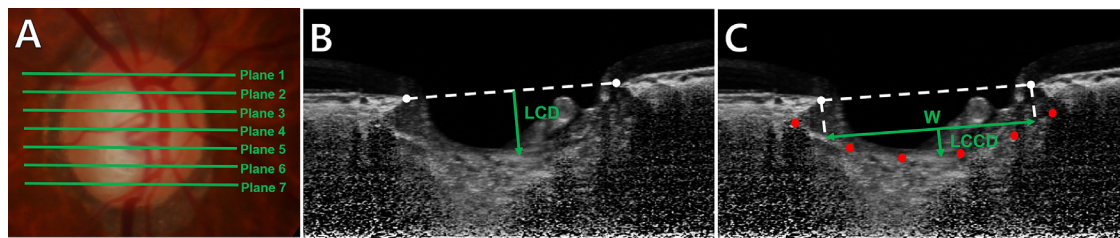
FIGURE 1. Measurements of LCD and LCCI. (**A**) Disc photograph showing seven horizontal *green lines* indicating the locations at which the measurements were taken. (**B**) Measurement of the LCD from the reference line connecting the two BMO points to the anterior surface of the LC. LCD was defined as the distance from this reference line at the maximally depressed point. (**C**) Determination of LCCI by dividing the LCCD within the BMO by the width of the anterior LC surface reference line (W), and then multiplying by 100.

diameter. The seven B-scan lines from the superior to the inferior regions were defined as planes 1 to 7 (Fig. 1A), with plane 4 corresponding to the midhorizontal plane, and planes 2 and 6 corresponding to the superior and inferior midperiphery planes, respectively. To determine the LCD, a line connecting the edges of the BMO was set as the reference plane (BMO reference line), and the LCD was measured in the direction perpendicular to the reference plane at the maximally depressed point (Fig. 1B).

LC Curve Measurement

The LC curves were assessed on EDI SD-OCT images, and LCCIs calculated as described.[44] In brief, LCCI was determined by measuring the width of the LC curve reference line (LCCW) and then measuring the LC curve depth (LCCD). The LCCW was defined as the width of the line connecting the two points on the anterior LC surface that met the lines drawn from each BMO termination point perpendicular to the BMO reference line. The maximum depth from the reference line to the anterior LC surface was defined as the LCCD (Fig. 1C). The LCCI was calculated as (LCCD/LCCW) X 100. Because the curvature is normalized relative to LC width, LCCI represents the shape of the LC independent of the actual size of the ONH. Only the LC within the BMO was considered because the LC outside the BMO was often not clearly visible. In eyes with LC defects, the LCCI and LCD were measured using a presumed anterior LC surface that best fit the curvature of the remaining part of the LC or excluded the area of the LC defect.

Data Analyses

Categorical variables were analyzed using the χ^2 test or the Fisher's exact test, as appropriate. The normality of continuous variables was analyzed by the Shapiro-Wilk test, and the equality of variances of these variables by the Levene's test. Variables in the three groups were compared by 1-way analysis of variance (ANOVA), Welch's ANOVA, and the Kruskal-Wallis rank-sum test were used to compare the continuous variables among three groups, followed by the Bonferroni's method of post hoc analysis for 1-way ANOVA and Kruskal-Wallis test or by the Games-Howell test for Welch's ANOVA. To conduct power analysis for unbalanced ANOVA and Kruskal-Wallis test, we performed the simulation. The power of the test for mean LCCI was 100%, and that for mean LCD was 99.98%. All analyses were two-tailed, with *P* values <0.05 considered statistically significant, except the Bonferroni's correction. All statistical analyses were performed with

SPSS version 25.0 (IBM Corp., Armonk, NY, USA) and R 3.6.3 (R Core Team, 2019).[55]

RESULTS

Baseline Characteristics

This study initially involved 29 patients diagnosed with ADOA. Of these, five patients were excluded because the image quality of their SD-OCT disc scans was too poor to allow clear visualization of their anterior LC surfaces. Twenty-four eyes of the remaining 24 ADOA patients, 11 men and 13 women, were enrolled. Of the 24 patients, the diagnosis was confirmed based on *OPA1* mutation in four patients, and the rest were diagnosed based on family history and clinical findings. Four patients received genetic evaluation for Leber's hereditary optic neuropathy, and the results were negative in all four patients. For comparison with ADOA group, 48 eyes of patients with NTG matched by age and global RNFL thickness and 48 eyes of 48 age-matched healthy control subjects were included.

Table 1 shows the clinical characteristics of these patients. CCT was significantly thinner in the NTG group than in the healthy control group (543.92 ± 31.39 vs. 560.19 ± 33.78 µm, *P* = 0.035). RNFL thickness was significantly thinner in the ADOA group (83.96 ± 8.05 µm) and NTG (83.28 ± 9.59 µm) group than in the healthy control group (103.48 ± 7.41 µm, *P* <0.001 each).

Comparison of LCD and LCCI

Measurements of LCCI and LCD showed excellent intraobserver reproducibility, with intraclass correlation coefficients of 0.968 (range, 0.958–0.977) for LCCI, and 0.965 (range, 0.945–0.978) for LCD.

Tables 2, 3 and Figure 2 show the measured LCCI and LCD values in each group. Mean LCCI was significantly higher in the NTG group (10.81 ± 2.97) than in the ADOA (6.09 ± 1.39) and control (6.69 ± 1.27) groups (*P* < 0.001 each). In addition, mean LCD was significantly higher in the NTG group (500.37 ± 118.97 µm) than in the ADOA (383.00 ± 85.39 µm) and normal control (405.88 ± 81.13 µm) groups (*P* < 0.001 each). The LCCIs in all seven planes were significantly higher in NTG than in ADOA and healthy control eyes (all *P* < 0.001).

REPRESENTATIVE CASES

Figure 3 shows a comparison of LCD and LCCI in an NTG eye and an ADOA eye.

TABLE 1. Demographic and Clinical Characteristics of the Study Subjects

| | | | | | Post Hoc Analysis | | |
Characteristics	Group 1 (n = 24)	Group 2 (n = 48)	Group 3 (n = 48)	_P_ Value	Group 1 vs. Group 2	Group 1 vs. Group 3	Group 2 vs. Group 3
Age, y	63.25 ± 15.66	63.42 ± 12.74	63.38 ± 14.45	0.894†			
Female, no. (%)	13 (54.17)	29 (58.00)	36 (75.00)	0.116‡			
IOP, mm Hg	13.17 ± 2.75	13.00 ± 2.98	12.90 ± 2.75	0.884†			
Spherical equivalent, D	–0.45 ± 1.64	–0.39 ± 1.85	0.37 ± 1.76	**0.026†**	0.624	0.022	0.025
Axial length, mm	23.89 ± 0.91	23.91 ± 1.22	23.52 ± 0.92	0.156†			
CCT, μm	557.00 ± 29.18	543.92 ± 31.39	560.19 ± 33.78	**0.036***	0.085	0.681	**0.015**
Disc area, mm²	2.18 ± 0.41	2.30 ± 0.40	2.29 ± 0.39	0.276†			
RNFL thickness, μm	83.96 ± 8.05	83.28 ± 9.59	103.48 ± 7.41	**<0.001***	0.751	**<0.001**	**<0.001**
History of diabetes mellitus, no. (%)	5 (20.83)	5 (10.00)	7 (14.58)	0.446‡			
History of hypertension, no. (%)	7 (29.17)	14 (28.00)	14 (29.17)	0.99‡			
History of thyroid disease, no. (%)	1 (4.17)	2 (4.00)	1 (2.08)	0.836§			

Data are mean ± standard deviation, with statistically significant _P_ values (<0.05) in boldface. Statistical significance was tested by *1-way ANOVA, †Kruskal-Wallis rank-sum test, ‡χ^2 test, or §Fisher's exact test. Bonferroni's method was applied for post hoc analyses in 1-way ANOVA and Kruskal-Wallis rank-sum test with statistically significant _P_ values (<0.017; 0.05/3) in boldface. Group 1 = eyes with ADOA; group 2 = eyes with NTG; group 3 = normal healthy eyes.

TABLE 2. LCCI in Eyes with ADOA, NTG, and in Healthy Eyes

| | | LCCI | | | | | |
| | | | | | Post Hoc Analysis | | |
Plane Number	Group 1 (n = 24)	Group 2 (n = 48)	Group 3 (n = 48)	_P_ Value	Group 1 vs. Group 2	Group 1 vs. Group 3	Group 2 vs. Group 3
1	6.92 ± 1.92	11.14 ± 3.62	7.42 ± 1.49	**<0.001***	**<0.001**	0.509	**<0.001**
2	6.78 ± 1.92	10.92 ± 3.38	7.22 ± 1.55	**<0.001***	**<0.001**	0.592	**<0.001**
3	5.77 ± 2.33	10.83 ± 3.60	6.41 ± 1.58	**<0.001†**	**<0.001**	0.170	**<0.001**
4	5.10 ± 2.14	10.15 ± 3.39	6.03 ± 1.66	**<0.001†**	**<0.001**	0.093	**<0.001**
5	5.13 ± 1.53	10.23 ± 3.39	6.26 ± 1.50	**<0.001†**	**<0.001**	0.043	**<0.001**
6	6.22 ± 1.78	10.87 ± 3.71	6.47 ± 1.40	**<0.001†**	**<0.001**	0.663	**<0.001**
7	6.71 ± 2.03	11.53 ± 3.60	7.04 ± 1.80	**<0.001†**	**<0.001**	0.557	**<0.001**
Mean	6.09 ± 1.39	10.81 ± 2.97	6.69 ± 1.27	**<0.001***	**<0.001**	0.184	**<0.001**

Data are mean ± standard deviation, with statistically significant _P_ values (<0.05) in boldface. Statistical significance was tested by *Welch's ANOVA, or †Kruskal-Wallis rank-sum test. Bonferroni's methods applied for post hoc analyses in the Kruskal-Wallis rank-sum test with statistically significant _P_ values (<0.017; 0.05/3) in boldface, and the Games-Howell test in Welch's ANOVA with statistically significant _P_ values (<0.05) in boldface. Group 1 = eyes with ADOA; group 2 = eyes with NTG; group 3 = healthy eyes.

TABLE 3. LCD in Eyes with ADOA, NTG, and in Healthy Eyes

| | | LCD | | | | | |
| | | | | | Post Hoc Analysis | | |
Plane Number	Group 1 (n = 24)	Group 2 (n = 48)	Group 3 (n = 48)	_P_ Value	Group 1 vs. Group 2	Group 1 vs. Group 3	Group 2 vs. Group 3
1	417.54 ± 91.06	534.94 ± 128.48	427.69 ± 90.88	**<0.001***	**<0.001**	0.658	**<0.001**
2	412.33 ± 91.13	540.74 ± 130.55	431.27 ± 88.35	**<0.001†**	**<0.001**	0.681	**<0.001**
3	384.71 ± 91.94	522.30 ± 133.36	419.52 ± 86.12	**<0.001†**	**<0.001**	0.280	**0.001**
4	366.96 ± 100.40	485.96 ± 123.41	403.88 ± 89.89	**<0.001***	**<0.001**	0.136	**0.001**
5	370.58 ± 99.38	476.44 ± 120.69	396.31 ± 92.98	**<0.001***	**<0.001**	0.296	**0.001**
6	368.08 ± 86.96	473.60 ± 112.67	384.38 ± 74.46	**<0.001***	**<0.001**	0.437	**<0.001**
7	360.79 ± 83.47	468.62 ± 115.70	378.08 ± 77.67	**<0.001†**	**<0.001**	0.676	**<0.001**
Mean	383.00 ± 85.39	500.37 ± 118.97	405.88 ± 81.13	**<0.001†**	**<0.001**	0.526	**<0.001**

Data are mean ± standard deviation, with statistically significant _P_ values (<0.05) in boldface.
Statistical significance was tested by *1-way ANOVA or †Welch's ANOVA.
Bonferroni's methods applied for post hoc analyses in 1-way ANOVA with statistically significant _P_ values (<0.017; 0.05/3) in boldface, and the Games-Howell test in Welch's ANOVA with statistically significant _P_ values (<0.05) in boldface.
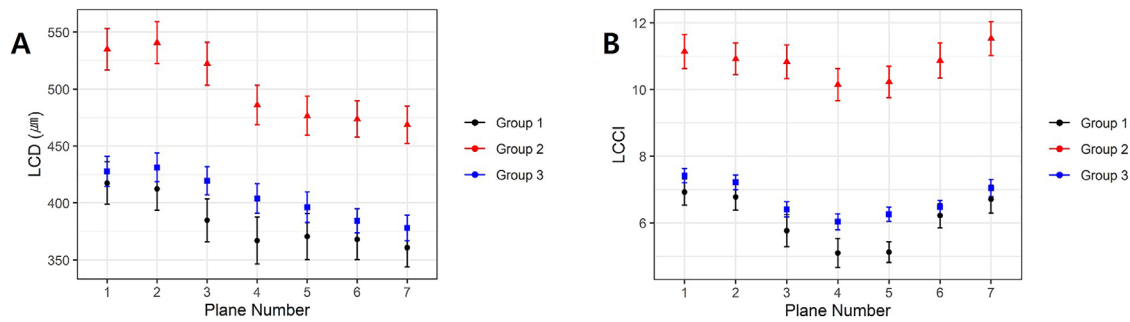Group 1 = eyes with ADOA; group 2 = eyes with NTG; group 3 = healthy eyes.

FIGURE 2. Variations in LCD (**A**) and LCCI (**B**) in the different planes and groups of patients, with groups 1, 2, and 3 representing the ADOA, NTG, and health control groups, respectively. *Error bars* indicate the standard error of the mean.
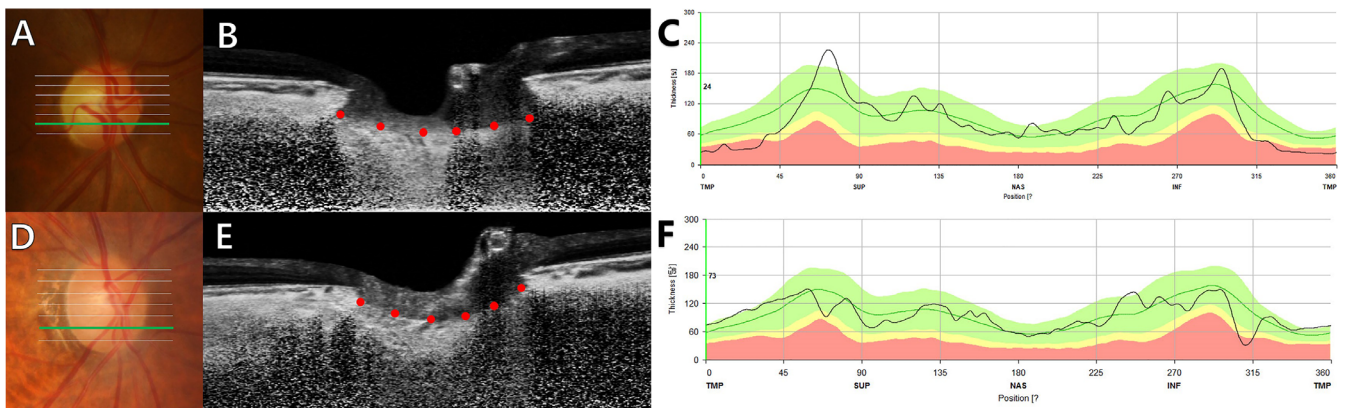

FIGURE 3. Representative eyes showing the LC morphology in (**A–C**) an eye with ADOA in a 72-year-old woman, and (**D–F**) an eye with NTG in a 77-year-old woman. (**A** and **D**) Optic disc photographs showing temporal pallor of the optic disc. (**B** and **E**) B-scan images at plane 6, indicated by the *green lines* in the optic disc photographs. (**C** and **F**) OCT circumpapillary scanning of the RNFL. (**C**) RNFL thickness reduction of the inferotemporal region. (**F**) RNFL thickness reduction in the temporal region.

DISCUSSION

This study found that ADOA eyes had less steeply curved LCs and smaller LCDs than NTG eyes. There were no significant differences in LCCI and LCD between ADOA and healthy control eyes. To our knowledge, no previous studies have compared LC morphology in ADOA eyes with morphology in NTG and healthy eyes.

The finding, that LCCI was greater in NTG than in healthy eyes, was in agreement with previous studies,[45,46] which showed that LCs were steeply curved in NTG patients. The stress caused by IOP induces posterior bowing of the LC.[19,47] Glaucoma is also characterized by posterior migration of the LC insertion,[48,49] which contributes to both greater LCD and posterior bowing.

Unlike other nonglaucomatous optic neuropathies, such as nonarteritic ischemic optic neuropathy and compressive optic neuropathy, patients with ADOA often experience excavation of the ONH, which can lead to a misdiagnosis of glaucoma.[9,11] In this study, mean LCCI and LCD did not differ significantly in the ADOA and healthy control groups, indicating that excavation of the ONH in ADOA was more likely because of the loss of prelaminar tissues than to deformation of the LC. Morphologically, the LC does not differ in ADOA and healthy control eyes, suggesting that this morphologic characteristic may be important in differentiating ADOA from NTG.

The LCCI at all planes differed significantly between the NTG and control groups, whereas LCD differed only at planes 1, 2, 6, and 7. This finding is consistent with the limited ability of LCDs to analyze LC deformation in glaucomatous eyes.[44] The LCD measured from the BMO is affected by choroidal thickness, which varies among individuals.[50]

It is unclear whether the LC morphology that differentiates glaucomatous from healthy eyes precedes or follows axonal loss. LC deformation was shown to occur prior to detectable changes in RNFL thickness, as measured by SD-OCT in a monkey glaucoma model.[20] In addition, previous findings indicate that large LCCI predicts a faster rate RNFL loss in patients suspected of having glaucoma,[51] suggesting that LC deformation precedes axonal loss. The results of the current study provide important insight into this issue.

The pathogenesis of ADOA involves retinal ganglion degeneration due to abnormal mitochondrial metabolism and impaired oxidative phosphorylation.[52,53] The present study also found that RNFL thickness was significantly lower in ADOA than in healthy eyes, whereas their LC features did not differ. This finding indicates that axonal loss does not trigger or induce LC deformation, indicating that glaucomatous LC deformation is not likely to be a secondary response to axonal loss.

This study had several limitations. First, some patients in the ADOA group were not diagnosed by genetic analysis of the *OPA1* gene. However, its autosomal-dominant inher-

itance was confirmed by taking a family history, and other clinical features characteristic of ADOA, including bilaterally symmetrical RNFL loss, especially in the temporal sector, were observed.[33] Therefore the possibility that NTG eyes were diagnosed as ADOA or vice versa was likely negligible. Second, only the LC inside the BMO width was included in measurements of LC curves because the LC outside the BMO width is often not visible. However, we found that LCCI measured using the entire LC, including the LC insertions, was comparable to that measured using the LC within the BMO,[54] suggesting that the LC curve inside the BMO is representative of the entire LC curve. Third, although we referred to the bowed LC configuration as the LC curvature, the LCCI does not correspond to the actual LC curvature but is only an approximation. Further studies are needed to investigate the optimal method of calculating the actual curvature of the LC. Finally, all subjects of this study were of Korean ethnicity, suggesting that our findings may not be applicable to other ethnic populations.

CONCLUSIONS

The present study found that the LC features differed significantly in ADOA and NTG eyes. These results provide insight into the differing pathogenesis of optic nerve damage in the two diseases. LC examination may be used as an adjunct to differentiate ADOA from NTG in ambiguous cases.

References

1. Thylefors B, Negrel AD, Pararajasegaram R, Dadzie KY. Global data on blindness. *Bull World Health Organ*. 1995;73:115–121.
2. O'Neill EC, Mackey DA, Connell PP, Hewitt AW, Danesh-Meyer HV, Crowston JG. The optic nerve head in hereditary optic neuropathies. *Nat Rev Neurol*. 2009;5:277–287.
3. Alexander C, Votruba M, Pesch UE, et al. *OPA1*, encoding a dynamin-related GTPase, is mutated in autosomal dominant optic atrophy linked to chromosome 3q28. *Nat Genet*. 2000;26:211–215.
4. Delettre C, Lenaers G, Griffoin JM, et al. Nuclear gene *OPA1*, encoding a mitochondrial dynamin-related protein, is mutated in dominant optic atrophy. *Nat Genet*. 2000;26:207–210.
5. Caldwell JB, Howard RO, Riggs LA. Dominant juvenile optic atrophy. A study in two families and review of hereditary disease in childhood. *Arch Ophthalmol*. 1971;85:133–147.
6. Hoyt CS. Autosomal dominant optic atrophy. A spectrum of disability. *Ophthalmology*. 1980;87:245–251.
7. Kline LB, Glaser JS. Dominant optic atrophy. The clinical profile. *Arch Ophthalmol*. 1979;97:1680–1686.
8. Jaeger W. Diagnosis of dominant infantile optic atrophy in early childhood. *Ophthalmic Paediatr Genet*. 1988;9:7–11.
9. Fournier AV, Damji KF, Epstein DL, Pollock SC. Disc excavation in dominant optic atrophy: differentiation from normal tension glaucoma. *Ophthalmology*. 2001;108:1595–1602.
10. Katz BJ. Disc excavation in dominant optic atrophy. *Ophthalmology*. 2002;109:1947; author reply 1947.
11. O'Neill EC, Danesh-Meyer HV, Kong GX, et al. Optic disc evaluation in optic neuropathies: the optic disc assessment project. *Ophthalmology*. 2011;118:964–970.
12. Votruba M, Thiselton D, Bhattacharya SS. Optic disc morphology of patients with *OPA1* autosomal dominant optic atrophy. *Br J Ophthalmol*. 2003;87:48–53.
13. Sung MS, Kang YS, Heo H, Park SW. Optic disc rotation as a clue for predicting visual field progression in myopic normal-tension glaucoma. *Ophthalmology*. 2016;123:1484–1493.
14. Kim MJ, Kim MJ, Kim HS, Jeoung JW, Park KH. Risk factors for open-angle glaucoma with normal baseline intraocular pressure in a young population: the Korea National Health and Nutrition Examination Survey. *Clin Exp Ophthalmol*. 2014;42:825–832.
15. Johnston RL, Seller MJ, Behnam JT, Burdon MA, Spalton DJ. Dominant optic atrophy. Refining the clinical diagnostic criteria in light of genetic linkage studies. *Ophthalmology*. 1999;106:123–128.
16. Bennett SR, Alward WL, Folberg R. An autosomal dominant form of low-tension glaucoma. *Am J Ophthalmol*. 1989;108:238–244.
17. Williams-Lyn D, Flanagan J, Buys Y, et al. The genetic aspects of adult-onset glaucoma: a perspective from the Greater Toronto area. *Can J Ophthalmol*. 2000;35:12–17.
18. Quigley HA, Addicks EM, Green WR, Maumenee AE. Optic nerve damage in human glaucoma. II. The site of injury and susceptibility to damage. *Arch Ophthalmol*. 1981;99:635–649.
19. Bellezza AJ, Rintalan CJ, Thompson HW, Downs JC, Hart RT, Burgoyne CF. Deformation of the lamina cribrosa and anterior scleral canal wall in early experimental glaucoma. *Invest Ophthalmol Vis Sci*. 2003;44:623–637.
20. He L, Yang H, Gardiner SK, et al. Longitudinal detection of optic nerve head changes by spectral domain optical coherence tomography in early experimental glaucoma. *Invest Ophthalmol Vis Sci*. 2014;55:574–586.
21. Anderson DR, Hendrickson A. Effect of intraocular pressure on rapid axoplasmic transport in monkey optic nerve. *Invest Ophthalmol*. 1974;13:771–783.
22. Minckler DS, Bunt AH, Johanson GW. Orthograde and retrograde axoplasmic transport during acute ocular hypertension in the monkey. *Invest Ophthalmol Vis Sci*. 1977;16:426–441.
23. Minckler DS, Tso MO. A light microscopic, autoradiographic study of axoplasmic transport in the normal rhesus optic nerve head. *Am J Ophthalmol*. 1976;82:1–15.
24. Hernandez MR. The optic nerve head in glaucoma: role of astrocytes in tissue remodeling. *Prog Retin Eye Res*. 2000;19:297–321.
25. Burgoyne CF, Downs JC, Bellezza AJ, Suh JK, Hart RT. The optic nerve head as a biomechanical structure: a new paradigm for understanding the role of IOP-related stress and strain in the pathophysiology of glaucomatous optic nerve head damage. *Prog Retin Eye Res*. 2005;24:39–73.
26. Roberts MD, Sigal IA, Liang Y, Burgoyne CF, Downs JC. Changes in the biomechanical response of the optic nerve head in early experimental glaucoma. *Invest Ophthalmol Vis Sci*. 2010;51:5675–5684.
27. Johnston PB, Gaster RN, Smith VC, Tripathi RC. A clinicopathologic study of autosomal dominant optic atrophy. *Am J Ophthalmol*. 1979;88:868–875.
28. Kjer P, Jensen OA, Klinken L. Histopathology of eye, optic nerve and brain in a case of dominant optic atrophy. *Acta Ophthalmol (Copenh)*. 1983;61:300–312.
29. Harding GF, Crews SJ, Pitts SM. Psychophysical and visual evoked potential findings in hereditary optic atrophy. *Trans Ophthalmol Soc U K*. 1979;99:96–102.

30. Berninger TA, Jaeger W, Krastel H. Electrophysiology and colour perimetry in dominant infantile optic atrophy. *Br J Ophthalmol*. 1991;75:49–52.

31. Holder GE. Significance of abnormal pattern electroretinography in anterior visual pathway dysfunction. *Br J Ophthalmol*. 1987;71:166–171.

32. Anderson DR, Patella VM. *Automated Static Perimetry*. 2nd ed. St. Louis: Mosby; 1999:xiv, 363.

33. Kim TW, Hwang JM. Stratus OCT in dominant optic atrophy: features differentiating it from glaucoma. *J Glaucoma*. 2007;16:655–658.

34. Alasil T, Wang K, Keane PA, et al. Analysis of normal retinal nerve fiber layer thickness by age, sex, and race using spectral domain optical coherence tomography. *J Glaucoma*. 2013;22:532–541.

35. Wu H, de Boer JF, Chen TC. Reproducibility of retinal nerve fiber layer thickness measurements using spectral domain optical coherence tomography. *J Glaucoma*. 2011;20:470–476.

36. Jonas JB, Papastathopoulos KI. Optic disc shape in glaucoma. *Graefes Arch Clin Exp Ophthalmol*. 1996;234(suppl 1):S167–S173.

37. Vongphanit J, Mitchell P, Wang JJ. Population prevalence of tilted optic disks and the relationship of this sign to refractive error. *Am J Ophthalmol*. 2002;133:679–685.

38. Samarawickrama C, Mitchell P, Tong L, et al. Myopia-related optic disc and retinal changes in adolescent children from Singapore. *Ophthalmology*. 2011;118:2050–2057.

39. Spaide RF, Koizumi H, Pozzoni MC. Enhanced depth imaging spectral-domain optical coherence tomography. *Am J Ophthalmol*. 2008;146:496–500.

40. Lee EJ, Kim TW, Weinreb RN, Park KH, Kim SH, Kim DM. Visualization of the lamina cribrosa using enhanced depth imaging spectral-domain optical coherence tomography. *Am J Ophthalmol*. 2011;152:87–95, e81.

41. Girard MJ, Tun TA, Husain R, et al. Lamina cribrosa visibility using optical coherence tomography: comparison of devices and effects of image enhancement techniques. *Invest Ophthalmol Vis Sci*. 2015;56:865–874.

42. Girard MJ, Strouthidis NG, Ethier CR, Mari JM. Shadow removal and contrast enhancement in optical coherence tomography images of the human optic nerve head. *Invest Ophthalmol Vis Sci*. 2011;52:7738–7748.

43. Mari JM, Strouthidis NG, Park SC, Girard MJ. Enhancement of lamina cribrosa visibility in optical coherence tomography images using adaptive compensation. *Invest Ophthalmol Vis Sci*. 2013;54:2238–2247.

44. Lee SH, Kim TW, Lee EJ, Girard MJ, Mari JM. Diagnostic power of lamina cribrosa depth and curvature in glaucoma. *Invest Ophthalmol Vis Sci*. 2017;58:755–762.

45. Kim JA, Kim TW, Lee EJ, Kim JM, Girard MJA, Mari JM. Intereye comparison of lamina cribrosa curvature in normal tension glaucoma patients with unilateral damage. *Invest Ophthalmol Vis Sci*. 2019;60:2423–2430.

46. Lee SH, Kim TW, Lee EJ, Girard MJA, Mari JM, Ritch R. Ocular and clinical characteristics associated with the extent of posterior lamina cribrosa curve in normal tension glaucoma. *Sci Rep*. 2018;8:961.

47. Yang H, Ren R, Lockwood H, et al. The connective tissue components of optic nerve head cupping in monkey experimental glaucoma part 1: global change. *Invest Ophthalmol Vis Sci*. 2015;56:7661–7678.

48. Yang H, Williams G, Downs JC, et al. Posterior (outward) migration of the lamina cribrosa and early cupping in monkey experimental glaucoma. *Invest Ophthalmol Vis Sci*. 2011;52:7109–7121.

49. Lee KM, Kim TW, Weinreb RN, Lee EJ, Girard MJ, Mari JM. Anterior lamina cribrosa insertion in primary open-angle glaucoma patients and healthy subjects. *PLoS One*. 2014;9:e114935.

50. Rhodes LA, Huisingh C, Johnstone J, et al. Peripapillary choroidal thickness variation with age and race in normal eyes. *Invest Ophthalmol Vis Sci*. 2015;56:1872–1879.

51. Kim JA, Kim TW, Weinreb RN, Lee EJ, Girard MJA, Mari JM. Lamina cribrosa morphology predicts progressive retinal nerve fiber layer loss in eyes with suspected glaucoma. *Sci Rep*. 2018;8:738.

52. Chun BY, Rizzo JF, 3rd. Dominant optic atrophy and Leber's hereditary optic neuropathy: update on clinical features and current therapeutic approaches. *Semin Pediatr Neurol*. 2017;24:129–134.

53. Chun BY, Rizzo JF, 3rd. Dominant optic atrophy: updates on the pathophysiology and clinical manifestations of the optic atrophy 1 mutation. *Curr Opin Ophthalmol*. 2016;27:475–480.

54. Lee SH, Yu DA, Kim TW, Lee EJ, Girard MJ, Mari JM. Reduction of the lamina cribrosa curvature after trabeculectomy in glaucoma. *Invest Ophthalmol Vis Sci*. 2016;57:5006–5014.

55. R Core Team 2019. R: A language and environment for statistical computing. R Foundation for Statistical Computing, Vienna, Austria. URL http://www.R-project.org/.